

Quantum metrology of low frequency electromagnetic modes with frequency upconverters

Stephen E. Kuenstner,¹ Elizabeth C. van Assendelft,¹ Saptarshi Chaudhuri,² Hsiao-Mei Cho,³ Jason Corbin,¹ Shawn W. Henderson,³ Fedja Kadribasic,¹ Dale Li,³ Arran Phipps,⁴ Nicholas M. Rapisdis,¹ Maria Simanovskaia,¹ Jyotirmai Singh,¹ Cyndia Yu,¹ and Kent D. Irwin^{1,3}

¹*Department of Physics, Stanford University, 382 Via Pueblo, Stanford, CA 94305.*

²*Department of Physics, Princeton University, Jadwin Hall Washington Road, Princeton, NJ 08544.*

³*SLAC National Accelerator Laboratory, 2575 Sand Hill Rd, Menlo Park, CA 94025*

⁴*Department of Physics, California State University East Bay, 25800 Carlos Bee Blvd, North Science 231, Hayward, CA 94542*

(Dated: July 2024)

We present the RF Quantum Upconverter (RQU) and describe its application to quantum metrology of electromagnetic modes between dc and the Very High Frequency band (VHF) ($\lesssim 300$ MHz). The RQU uses a Josephson interferometer made up of superconducting loops and Josephson junctions to implement a parametric interaction between a low-frequency electromagnetic mode (between dc and VHF) and a mode in the microwave C Band (~ 5 GHz), analogous to the radiation pressure interaction between electromagnetic and mechanical modes in cavity optomechanics. We analyze RQU performance with quantum amplifier theory, and show that the RQU can operate as a quantum-limited op-amp in this frequency range. It can also use non-classical measurement protocols equivalent to those used in cavity optomechanics, including back-action evading (BAE) measurements, sideband cooling, and two-mode squeezing. These protocols enable experiments using dc-VHF electromagnetic modes as quantum sensors with sensitivity better than the Standard Quantum Limit (SQL). We demonstrate signal upconversion from low frequencies to microwave C band using an RQU and show a phase-sensitive gain (extinction ratio) of 46.9 dB, which is a necessary step towards the realization of full BAE.

I. INTRODUCTION

The field of Circuit Quantum Electrodynamics (Circuit QED) has made impressive strides in harnessing the quantum-mechanical properties of superconducting circuits operating in the microwave frequency regime (typically several GHz) [1]. The techniques of Circuit QED have advanced to the point that detecting [2, 3] and coherently manipulating [4] a single microwave quantum are routine operations, and individual control over arrays of dozens of interacting quantum circuits is possible [5]. Much of this progress has been driven by the desire to build a universal quantum computer capable of performing calculations that would be impractical on any classical computer.

The techniques of Circuit QED do not extend directly to lower frequencies, however. Recently, there has been growing interest in adapting quantum metrology techniques to lower frequency electromagnetic modes, typically at frequencies between dc and the Very High Frequency (VHF) band below 300 MHz. Quantum metrology of low-frequency modes could offer a sensitivity advantage over classical sensors, enabling experiments including dark-matter searches [6], low-frequency nuclear spin metrology [7], some astronomical measurements [8], and low-frequency magnetometry, outperforming a dc SQUID in certain applications.

One approach for quantum RF metrology that has been developed at these frequencies is to use a qubit to cool the MHz resonator to its ground state and stabilize a Fock state with a small number of photons [9]. While this

approach can be used in principle to measure individual signal photons entering the resonator, it does not provide a way to discriminate incoming signal photons from background thermal photons, which limits its usefulness for certain measurements.

For example, searches for axion or axion-like dark matter at mass below 1 μ eV must detect or rule out yoctowatt-scale or smaller electromagnetic signals over many decades in frequency, spanning from ~ 100 Hz to ~ 300 MHz [6, 10–15]. These signals can be used to excite an electromagnetic resonator. If the photon number state of the resonator is then measured, the signal-to-noise ratio is limited by the random entry or departure of background thermal photons from the resonator, since photon-counting techniques lack the frequency resolution to distinguish thermal and signal photons. An alternative approach that applies quantum techniques to measure the dark-matter-induced voltage, rather than the photon number, allows the signal frequency to be determined. Frequency information is important as these circuits carry useful information significantly detuned from their resonant frequency. Far from the resonant frequency, thermal fluctuations are suppressed to below the level of a single photon per second per Hz of bandwidth [16, 17]. This off-resonant signal information can be accessed using continuous-variables readout techniques operating beyond the Standard Quantum Limit (SQL). In this case, improving the readout performance does not substantially improve the signal to noise ratio (SNR) on resonance (which is limited by thermal fluctuations), but it allows constant SNR to be maintained over a much

broader bandwidth, dramatically increasing the axion search rate.

In this work, we describe the RF Quantum Up-converter (RQU), a device that mimics the radiation-pressure interaction in cavity optomechanics, but replaces the low-frequency mechanical mode with a low-frequency electromagnetic mode. The RQU uses the nonlinearity of Josephson junctions to upconvert signals from the sensor frequency to microwave frequencies using a three-wave mixing interaction. We experimentally demonstrate three-wave mixing with an RQU in §VI.

This upconversion paradigm allows the RQU to take advantage of several mature microwave Circuit QED technologies, including high coherence microwave resonators [18], Josephson Parametric Amplifiers (JPAs) [19], and microwave squeezers [20], while extending the frequency range of quantum measurement techniques to lower frequencies. They also enable the use of quantum-limit evading techniques equivalent to those used in cavity optomechanics, including back-action evading (BAE) measurements [21]. After analyzing BAE using the RQU, in §VI we experimentally demonstrate a phase-sensitive gain of 46.9 dB, which is a significant step towards the realization of full BAE.

II. ANALOGY BETWEEN CAVITY OPTOMECHANICS AND OP-AMP MODE AMPLIFICATION

A. Upconverter Hamiltonian

To evaluate the RQU as a tool for quantum metrology, we use a model in which both the RQU and its input circuit are quantized, with an interaction Hamiltonian that couples the modes. This Hamiltonian is exactly analogous to that of cavity optomechanics, but the mechanical mode is replaced with an electromagnetic mode, referred to in this section as the “low-frequency mode” to distinguish it from the microwave mode.

Cavity optomechanics treats two bosonic modes at different frequencies: an electromagnetic mode at ω_a and a mechanical mode at ω_b , with $\omega_a \gg \omega_b$ [22]. The position operator of the mechanical mode represents the position of a movable mirror that forms one end of the optical cavity. The modes are quantized with ladder operators \hat{a} , \hat{a}^\dagger and \hat{b} , \hat{b}^\dagger , respectively. The uncoupled Hamiltonian is:

$$\hat{H}_0 = \hbar\omega_a(\hat{a}^\dagger\hat{a} + 1/2) + \hbar\omega_b(\hat{b}^\dagger\hat{b} + 1/2), \quad (1)$$

In terms of ladder operators, the mirror position is given by:

$$\hat{x} = x_{\text{ZPF}}(\hat{b} + \hat{b}^\dagger), \quad (2)$$

where x_{ZPF} is the magnitude of the zero-point position fluctuations. The frequency of photons occupying the op-

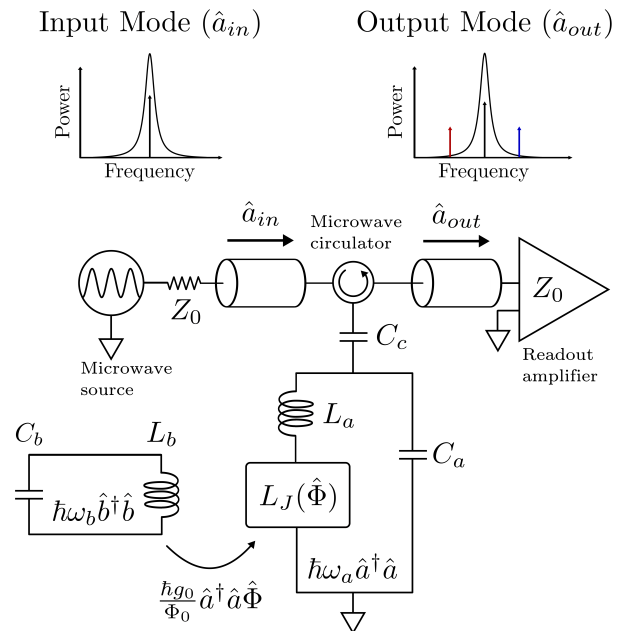


FIG. 1. A circuit model for an RQU, which inductively couples a dc-VHF signal source (shown here as a resonator formed by C_b and L_b) to a tunable Josephson inductance $L_J(\hat{\Phi})$. The tunable inductor is made up of a superconducting interferometer with one or more Josephson junctions (JJs) and one or more loops. The flux Φ threading the inductor L_b associated with the low-frequency mode also couples through a designable mutual inductance to each of the loops in the JJ interferometer. Thus, $\hat{\Phi}$ changes the inductance L_J presented by the JJ interferometer to the microwave mode, and modifies the resonance frequency of the microwave resonator formed by the interferometer and linear reactances modeled by circuit elements C_a and L_a . A coupling capacitance C_c , microwave transmission lines and a circulator allow the state of the microwave resonator to be driven and detected via traveling wave modes \hat{a}_{in} and \hat{a}_{out} , respectively. The output mode contains information in sidebands, as shown schematically in the frequency domain. Low noise amplification by a cryogenic microwave amplifier allows for efficient detection of the output state \hat{a}_{out} .

tical mode depends on the position of the movable mirror, leading to the parametric optomechanical interaction $\hat{H}_{\text{int}}^{\text{OM}}$ between the two modes:

$$\hat{H}_{\text{int}}^{\text{OM}} = -\frac{\hbar g_0}{x_{\text{ZPF}}} \hat{a}^\dagger \hat{a} \hat{x}, \quad (3)$$

where g_0 is the optomechanical coupling strength, describing the frequency shift of an optical photon due to the position \hat{x} of the mechanical oscillator.

An optomechanical-style coupling can be realized in microwave superconducting resonant circuits by including a Josephson interferometer whose inductance $L_J(\hat{\Phi})$ depends on the flux $\hat{\Phi}$ in the low-frequency mode. The flux causes the microwave resonance frequency to vary, just as position shifts of the moving mirror cause the

optical frequency to vary in the optomechanical setup. This optomechanical-style coupling has been realized in the microwave SQUID multiplexer [23] although not optimized to approach quantum limits. The dispersive nanoSQUID magnetometer [24] uses a similar frequency-tunable microwave resonator, but does not use a resonant low-frequency circuit on its input, removing the effects of quantum backaction and limiting the quantum protocols which could be employed. There are also other devices in which a resonator is tuned with a Josephson junction array, including the Asymmetrically Threaded SQUID (ATS) [25]. However, in the ATS, the lower frequency signal and higher frequency signal are both coupled as a current drive to the interferometer, and a flux input is used to bias and pump the interferometer for degenerate four-wave mixing. In the RQU, which uses optomechanical-style coupling, the low-frequency signal is applied as a flux to the Josephson interferometer and three-wave mixing is realized. Figure 1 shows a circuit model of such an upconverter with the associated ladder operators.

The uncoupled Hamiltonian of the RQU is exactly the one in equation 1, with the phonon ladder operators \hat{b}, \hat{b}^\dagger replaced by photon operators for the low-frequency mode. The microwave and low-frequency modes are represented by harmonic oscillators with frequencies:

$$\omega_a(\hat{\Phi}) = ((L_a + L_J(\hat{\Phi}))(C_a + C_c))^{-\frac{1}{2}}, \quad (4)$$

$$\omega_b = (L_b C_b)^{-\frac{1}{2}}. \quad (5)$$

The low frequency mode is inductively coupled to the Josephson interferometer such that the flux threading the low-frequency resonator also threads the Josephson interferometer. Arrays of multiple Josephson junctions and multiple loops can be used with both gradiometric and non-gradiometric coupling to optimize circuit response for different applications. The tunability of $L_J(\hat{\Phi})$ mediates a parametric interaction, with $\hat{\Phi}$ playing the role of the position operator \hat{x} . Analogously to equation 2, we have:

$$\hat{\Phi} = \Phi_{ZPF}(\hat{b} + \hat{b}^\dagger), \quad (6)$$

where Φ_{ZPF} is magnitude of the zero point flux fluctuations: $\Phi_{ZPF} = \sqrt{\hbar\omega_b L_b/2}$.

In order to treat the interaction between the modes, we include the perturbation of L_J due to the sensor flux. For small fluxes satisfying $|\hat{\Phi}| \ll \Phi_0$, we Taylor expand the microwave frequency to first order in the sensor flux, to calculate the shift of the microwave resonance frequency due to flux in the sensor:

$$\hat{H} = \hbar \left(\omega_a(0) + \frac{d\omega_a}{d\Phi} \hat{\Phi} \right) (\hat{a}^\dagger \hat{a} + 1/2) + \hbar\omega_b (\hat{b}^\dagger \hat{b} + 1/2). \quad (7)$$

The frequency shift per unit applied flux describes the

strength of the interaction between the modes, with:

$$\frac{d\omega_a}{d\Phi} = \frac{d\omega_a}{dL_J} \frac{dL_J}{d\Phi}. \quad (8)$$

The two derivatives on the RHS of equation 8 depend on the particular design of the interferometer and low frequency resonator, which we can calculate for a given interferometer design. We can write the upconverter interaction Hamiltonian in equation 7 in a form analogous to the radiation pressure interaction in equation 3:

$$\hat{H}_{int}^{RQU} = -\frac{\hbar g_0}{\Phi_{ZPF}} \hat{a}^\dagger \hat{a} \hat{\Phi} = -\hbar g_0 \hat{a}^\dagger \hat{a} (\hat{b}^\dagger + \hat{b}). \quad (9)$$

Without loss of generality, we choose the the sign of increasing $\hat{\Phi}$ to yield the minus sign in equation 7. Because it involves products of three ladder operators, this interaction describes three-wave mixing. The strength of the optomechanical-style coupling is given by:

$$g_0 \equiv \frac{d\omega_a}{d\Phi} \Phi_{ZPF}. \quad (10)$$

B. Input-Output Model

In order to operate the RQU, we control and detect the state of the microwave resonator, which allows us to infer the state of the low-frequency resonator. The Hamiltonian in equation 7 only accounts for the interaction between the two modes, and does not include external couplings or dissipation. In order to detect and control the state of the microwave resonator, we couple the microwave resonator to a waveguide that allows microwave photons to escape the cavity for amplification and demodulation. Finally, the model must also account for the effects of internal dissipation in both the RF and microwave modes.

The total Hamiltonian, accounting for the external coupling, dissipation, and the microwave drive is given by:

$$\hat{H}_{tot} = \hat{H}_0 + \hat{H}_{int} + \hat{H}_\kappa + \hat{H}_\gamma + \hat{H}_{drive}, \quad (11)$$

where $\hat{H}_0 + \hat{H}_{int}$ describes the dynamics of the isolated RQU system (microwave resonator plus low-frequency resonator, and their interaction), as described in equations 1 and 7. \hat{H}_κ captures the effects of loss in the microwave resonator, which is dominated by loss to the strongly coupled readout port. \hat{H}_γ describes loss to internal dissipation in the low-frequency resonator. Finally, \hat{H}_{drive} accounts for the energy supplied by the external drive tones which probe the RQU state.

The traveling-wave modes used in this section are shown in figure 1: the microwave resonator is coupled to an “input” mode \hat{a}_{in} and an “output” mode \hat{a}_{out} which are used to drive and detect the state of the microwave

resonator. The field circulating within the microwave resonator, \hat{a} , is referred to as the intra-cavity field. A circulator prevents leftward-propagating modes from interacting with the RQU, so we ignore them. The internal dissipation in the low-frequency resonator is modeled as arising from a semi-infinite transmission line of characteristic impedance R_b . The incident and reflected modes on this transmission line are \hat{b}_{in} and \hat{b}_{out} , respectively.

The noise fluctuations in these input and output modes can be analyzed using standard input-output theory [26], following a treatment similar to Section IIIB of [22]. The Heisenberg-Langevin equations of motion for the system are:

$$\dot{\hat{a}} = \frac{i}{\hbar} \left[\hat{H}_0 + \hat{H}_{int}, \hat{a} \right] - \frac{\kappa}{2} \hat{a} - \sqrt{\kappa} \hat{a}_{in}, \quad (12)$$

$$\dot{\hat{b}} = \frac{i}{\hbar} \left[\hat{H}_0 + \hat{H}_{int}, \hat{b} \right] - \frac{\gamma}{2} \hat{b} - \sqrt{\gamma} \hat{b}_{in}, \quad (13)$$

where κ is the decay rate of the circulating power in the microwave resonator, and γ is the decay rate in the low-frequency resonator. Dots indicate time derivatives. \hat{H}_{int} describes three-wave mixing, so equations 12 and 13 are nonlinear. Our present analysis will focus on the regime where we can linearize \hat{H}_{int} , although experiments in the highly nonlinear regime (when the single-photon interaction rate g_0 exceeds the microwave loss rate κ) are also interesting. To linearize, we write the microwave ladder operators as a sum of a classical amplitude and small quantum fluctuations:

$$\hat{a} = \bar{a} + \delta\hat{a}, \quad (14)$$

$$\hat{a}_{in} = \bar{a}_{in} + \delta\hat{a}_{in}, \quad (15)$$

$$\hat{a}_{out} = \bar{a}_{out} + \delta\hat{a}_{out}. \quad (16)$$

Here, $|\bar{a}|^2$ represents the average photon number circulating in the microwave resonator due to the drive. The drive has an amplitude $|\bar{a}_{in}|^2$ (in units of photons/second). Likewise, the average photon flux propagating towards the microwave amplifier is given by $|\bar{a}_{out}|^2$. The boundary condition relating the output, input, and intra-cavity fields is:

$$(\hat{a}_{out} - \hat{a}_{in}) = \sqrt{\kappa} \hat{a} \quad (17)$$

We operate the upconverter in the regime of strong microwave drives, such that $\bar{a} \gg 1$. Inserting expression 14 into the interaction Hamiltonian 7 yields:

$$\hat{H}_{int} = -\hbar g_0 (|\bar{a}|^2 + \bar{a}^* \delta\hat{a} + \bar{a} \delta\hat{a}^\dagger + \delta\hat{a}^\dagger \delta\hat{a}) (\hat{b}^\dagger + \hat{b}). \quad (18)$$

The first term represents a constant flux offset applied to the low-frequency resonator, and can be ignored. The second and third terms represent mixing between the coherent microwave amplitudes \bar{a}^* and \bar{a} and the quantum noise terms $\delta\hat{a}$ and $\delta\hat{a}^\dagger$. The last term represents the interaction of the quantum noise with itself, and since it is smaller than the second and third terms by a factor of $1/|\bar{a}| \ll 1$, we ignore it. Thus, the relevant portions of

the interaction Hamiltonian are:

$$\hat{H}_{int} \approx -\hbar g_0 (\bar{a}^* \delta\hat{a} + \bar{a} \delta\hat{a}^\dagger) (\hat{b}^\dagger + \hat{b}). \quad (19)$$

Since \bar{a} is a classical value rather than an operator, this interaction now describes an effective two-wave interaction with a tunable strength set by $g_0 |\bar{a}|$, rather than the three-wave interaction described by equation 7. Hence, we refer to it as the linearized interaction.

In order for \bar{a} to have a non-zero value in the steady state, external energy must be supplied to the microwave resonator via a driving term. A monotonic, coherent drive tone applied via the readout waveguide induces the drive Hamiltonian:

$$\hat{H}_{drive} = -i\hbar\sqrt{\kappa}(\bar{a}_{in}(t)\hat{a}^\dagger + \bar{a}_{in}^*(t)\hat{a}), \quad (20)$$

where $\bar{a}_{in}(t)$ represents the (classical) amplitude of the coherent voltage drive applied to the microwave resonator via the input transmission line. We apply the unitary transformation:

$$\hat{H}_{rot} = \hat{U} \hat{H}_{lab} \hat{U}^\dagger - i\hat{U} \dot{\hat{U}}^\dagger, \quad (21)$$

to move to a frame rotating at the drive frequency. $\hat{U} = \exp(i\omega_d \hat{a}^\dagger \hat{a} t)$, where ω_d is the angular velocity of the rotating frame. In this frame, the Heisenberg-Langevin equation of motion for \hat{a} reads:

$$\dot{\hat{a}} = \frac{i}{\hbar} \left[-\hbar \left(\Delta + \hbar g_0 (\hat{b}^\dagger + \hat{b}) \right) \hat{a}^\dagger \hat{a}, \hat{a} \right] - \frac{\kappa}{2} \hat{a} - \sqrt{\kappa} \hat{a}_{in}, \quad (22)$$

where $\Delta \equiv \omega_d - \omega_a$.

We begin by solving for the steady-state amplitude \bar{a} using the classical portion of the equation of motion 22, neglecting terms of order $\delta\hat{a}$ and with no flux applied from the sensor: $\hat{\Phi} = 0$. We find:

$$\bar{a} = \frac{\sqrt{\kappa} \bar{a}_{in}}{i\Delta - \frac{\kappa}{2}}. \quad (23)$$

We can insert this steady state classical amplitude into equations 13 and 22 in order to describe the linearized dynamics of the coupled modes in the frequency domain. After neglecting DC terms and small terms of order $\delta\hat{a}\hat{b}$, we find:

$$\begin{aligned} -i\omega\delta\hat{a}[\omega] &= (i\Delta - \kappa/2)\delta\hat{a}[\omega] - \\ &ig_0\bar{a}(\hat{b}^\dagger[\omega] + \hat{b}[\omega]) - \sqrt{\kappa}\delta\hat{a}_{in}[\omega] \end{aligned} \quad (24)$$

for the intra-cavity field, and

$$\begin{aligned} -i\omega\hat{b}[\omega] &= (-i\omega_b - \gamma/2)\hat{b}[\omega] - \\ &ig_0(\bar{a}^*\delta\hat{a}[\omega] + \bar{a}\delta\hat{a}^\dagger[\omega]) - \sqrt{\gamma}\hat{b}_{in}[\omega] \end{aligned} \quad (25)$$

for the low-frequency mode.

Equations 24 and 25 fully describe the dynamics of the

RQU in the linearized regime, and can be used to calculate the behavior of the coupled modes in a variety of regimes. The quantum metrology techniques in the following sections arise from special cases of these linearized dynamics where the detuning takes on the specific values $\Delta = 0$ or a superposition of drive tones at $\Delta = \pm\omega_b$.

C. Quantum amplifier theory

When the RQU is driven by a single microwave tone, it functions as a phase-preserving [27] electromagnetic amplifier that measures both the low-frequency signal quadratures with equal sensitivity. It is an op-amp mode amplifier [28] in the sense that it measures an input state variable (flux) in a lumped-element circuit rather than a traveling wave on a transmission line. The RQU maps the flux variable $\hat{\Phi}$ of the low-frequency circuit onto the microwave output mode $\delta\hat{a}_{out}$.

The upconversion process adds noise as required by the Standard Quantum Limit on amplification, and in this section we show that the RQU can achieve readout at the SQL [28]. In this readout protocol, the microwave readout tone is resonant ($\Delta = 0$), and the low frequency signal appears in $\delta\hat{a}_{out}$ as symmetric sidebands due to the phase modulation of the reflected microwave signal, which is a three-wave mixing process.

In order to evaluate the total noise added in the upconversion process, we calculate fluctuations in the output mode $\delta\hat{a}_{out}$. We use the boundary condition in equation 17 to eliminate the intra-cavity field in equation 24, yielding the equation of motion governing the small quantum fluctuations of the input and output microwave modes, and the low frequency mode:

$$\delta\hat{a}_{out}[\omega] = \frac{i\omega - \kappa/2}{i\omega + \kappa/2} \delta\hat{a}_{in}[\omega] + \frac{ig_0\bar{a}\sqrt{\kappa}}{(i\omega + \kappa/2)\Phi_{ZPF}} \hat{\Phi}[\omega]. \quad (26)$$

The first term on the RHS of equation 26 represents the fluctuations in the input mode, which are reflected from the microwave resonator with a phase shift, but no change in amplitude. These fluctuations carry no information about the state of the low-frequency resonator, and cause uncertainty in $\hat{\Phi}$, referred to as imprecision noise. The second term carries information about the state of the low-frequency resonator encoded in sidebands at $\pm\omega$ (in the rotating frame).

The other irreducible noise source arises from fluctuations in the intra-cavity field $\delta\hat{a}$ which perturb the state of the low-frequency resonator. Inserting the steady state solution for the intra-cavity field into equation 13 and focusing on the backaction terms yields an equation of motion for the low-frequency mode:

$$\hat{\delta}[\omega] = \left(i\omega_b - i\omega + \frac{\gamma}{2}\right)^{-1} \frac{ig_0\bar{a}}{\sqrt{\kappa}} (\delta\hat{a}^\dagger[\omega] + \delta\hat{a}[\omega]), \quad (27)$$

where (without loss of generality) we have set the phase

of a_{in} so that \bar{a} is real. Equation 27 captures the effects of microwave fluctuations that perturb the state of the low-frequency resonator, including backaction due to fluctuations in the microwave field (proportional to $\delta\hat{a}$ and $\delta\hat{a}^\dagger$). Together, equations 26 and 27 describe the two irreducible noise sources in the upconversion process. Since the RQU is functioning as an op-amp (meaning that it measures a state variable rather than a traveling wave), it is more convenient to describe the noise in the upconversion process directly in terms of the voltages and currents in the low-frequency resonator.

We take the limit of low frequencies, where the generated sidebands are within the bandwidth of the microwave resonator, $\omega \ll \kappa/2$. The total output signal at the follow-on microwave amplifier is given by equation 16. In order to recover the flux signal, we noiselessly amplify (with a degenerate JPA) and demodulate using a reference tone at ω_d , measuring the microwave phase quadrature $\hat{a}_{out}[\omega] - \hat{a}_{out}^\dagger[\omega]$:

$$\hat{a}_{out}[\omega] - \hat{a}_{out}^\dagger[\omega] = \delta\hat{a}_{in}[\omega] - \delta\hat{a}_{in}^\dagger[\omega] + \frac{4ig_0\bar{a}}{\sqrt{\kappa}} \frac{\hat{\Phi}[\omega]}{\Phi_{ZPF}}. \quad (28)$$

The imprecision fluctuations can be referred back to input currents with equation 28, yielding:

$$\hat{I}_{imp} = \frac{\Phi_{ZPF}\sqrt{\kappa}}{4ig_0M\bar{a}} \left(\delta\hat{a}_{in}[\omega] - \delta\hat{a}_{in}^\dagger[\omega]\right), \quad (29)$$

where M is the effective mutual inductance relating the input flux signal $\hat{\Phi}$ to \hat{I} , the current flowing through L_b .

Using the backaction terms in equation 27, we can write the perturbation of the low-frequency current due to backaction. We find:

$$\hat{I}_{BA}[\omega] = (Y_+[\omega] + Y_-[\omega]) \hat{V}_{BA}[\omega], \quad (30)$$

where $Y_\pm[\omega]$ is approximately the admittance of the low-frequency resonator at its positive and negative resonance frequencies:

$$Y_\pm[\omega] = \frac{1}{2iL_b(i\gamma/2 - \omega \pm \omega_b)} \quad (31)$$

The approximation in equation 31 holds for frequencies near the resonance frequencies $\omega \approx \pm\omega_b$. In order to evaluate the effect of backaction at frequencies very detuned from the resonance frequency, the rotating wave approximation implicit in the derivation of equation 13 would have to be dropped. The backaction voltage $\hat{V}_{BA}[\omega]$ arises from the fluctuation terms $\delta\hat{a}$ and $\delta\hat{a}^\dagger$, and is given by:

$$\hat{V}_{BA}[\omega] = \frac{8i\omega M g_0 Q_{ZPF} |\bar{a}|}{\kappa} (\delta\hat{a}[\omega] + \delta\hat{a}^\dagger[\omega]), \quad (32)$$

Equations 32 and 29 show the backaction and imprecision noise contributions arise from the input quadratures

$\hat{\delta}_{BA} = \delta\hat{a}_{in}[\omega] + \delta\hat{a}_{in}^\dagger[\omega]$ and $\hat{\delta}_{imp} = \delta\hat{a}_{in}[\omega] - \delta\hat{a}_{in}^\dagger[\omega]$, respectively. If the input is prepared in a coherent state without additional noise and the output mode is detected without adding noise (e.g. if $\delta\hat{a}_{in}, \delta\hat{a}_{in}^\dagger$, are sourced from a cold resistor, and a noiseless, phase-sensitive JPA detects $\delta\hat{a}_{out}, \delta\hat{a}_{out}^\dagger$), the fluctuations of these mode quadratures are described by the (symmetrized) noise spectral densities:

$$\bar{S}_{\delta_{BA}\delta_{BA}}[\omega] = 1, \quad (33)$$

$$\bar{S}_{\delta_{imp}\delta_{imp}}[\omega] = 1, \quad (34)$$

$$\bar{S}_{\delta_{BA}\delta_{imp}}[\omega] = 0, \quad (35)$$

In other words, the quadratures have uncorrelated fluctuations with a total amplitude corresponding to a single quantum. We can now evaluate the imprecision and backaction spectral densities:

$$\bar{S}_{II} = \frac{\Phi_{ZPF}^2 \kappa}{8|\bar{a}|^2 g_0^2 M^2}, \quad (36)$$

$$\bar{S}_{VV} = \frac{8|\bar{a}|^2 g_0^2 M^2 \omega^2 Q_{ZPF}^2}{\kappa}, \quad (37)$$

$$\bar{S}_{IV} = 0. \quad (38)$$

These spectral densities describe an op-amp mode amplifier operating at the Standard Quantum Limit for a phase-preserving amplifier. The noise impedance of this amplifier is tunable without changing the geometry or input inductance of the device, simply by changing the microwave amplitude $|\bar{a}|$. The total noise added by such an amplifier is the sum of these three contributions, with the op-amp achieving a total added current noise of:

$$\bar{S}_{II,tot} = \bar{S}_{II} + \bar{S}_{VV} |\bar{Y}[\omega]|^2 + 2\text{Re}(\bar{S}_{IV} \bar{Y}[\omega]^*), \quad (39)$$

where $\bar{Y}[\omega] = Y_+[\omega] + Y_-[\omega]$ is the sum of the positive- and negative-frequency components of the admittance. On resonance at $\omega = \omega_b$, the admittance is purely real: $\bar{Y}[\omega_b] = 1/R_b$. Using also the fact that $S_{IV} = 0$, we can simplify the total noise to:

$$2k_B T_N[\omega_b] = \frac{\bar{S}_{VV}}{R_b} + R_b \bar{S}_{II}, \quad (40)$$

where $T_N[\omega]$ is the noise temperature, which is a function of the frequency, evaluated on resonance at $\omega = \omega_b$. Note that the densities in equations 36 and 37 have different scalings with respect to the microwave drive power $|a|$. Thus, for the simplified case of optimizing the added noise on resonance, with $\Delta = 0$, we find that the real, on-resonance input circuit resistance R_{noise} (the ‘‘noise impedance’’) that optimizes the noise temperature is

$$R_{\text{noise}} = \sqrt{\frac{S_{VV}}{S_{II}}} = \frac{8|\bar{a}|^2 g_0^2 \omega M^2 Q_{ZPF}}{\kappa}. \quad (41)$$

So, the noise resistance of the RQU can be tuned by changing the pump power $|\bar{a}|^2$, without changing the in-

put inductance.

The noise temperature is optimized when $R_b = R_{\text{noise}}$. We find the optimal power level is given by:

$$|\bar{a}|^2 = \frac{R_b \kappa}{8g_0^2 M^2 \omega} \frac{Q_{ZPF}}{\Phi_{ZPF}}, \quad (42)$$

with an overall noise temperature of:

$$k_B T_N[\omega_b] = \frac{\hbar \omega_b}{2} \quad (43)$$

This corresponds to an op-amp mode amplifier operating at the SQL.

In reality, we cannot operate the RQU at arbitrarily high microwave drive levels. The upper limit on the value of $|\bar{a}_{in}|^2$ will be set by nonlinear terms in the Josephson inductance, leading to Kerr-type nonlinearity, where the effective inductance of the interferometer is a function of amplitude of the currents circulating in the microwave resonator. This introduces terms of the form:

$$\hat{H}_{Kerr} = \hbar \Lambda \hat{a}^\dagger \hat{a}^\dagger \hat{a} \hat{a}, \quad (44)$$

where Λ quantifies the strength of the quartic nonlinearity in the microwave circuit. Kerr-type nonlinearity has been extensively studied in the context of parametric amplifiers, but the most relevant effect for the RQU is the microwave power-dependent frequency shift. At high microwave powers, this frequency shift causes the microwave resonator to bifurcate. This imposes an upper limit on the microwave power circulating within the RQU [29]:

$$|\bar{a}_{max}|^2 = \chi |\bar{a}_{bif}|^2 = \frac{1}{2\sqrt{3}} \frac{\kappa}{\Lambda}, \quad (45)$$

where $\chi \lesssim 1$ sets how far below the onset of bifurcation the RQU is operated. This limits the highest noise resistance R_{max} that can be achieved:

$$R_{max} = \sqrt{\frac{S_{VV}}{S_{II}}} = \frac{8|\bar{a}_{max}|^2 g_0^2 \omega M^2 Q_{ZPF}}{\kappa \Phi_{ZPF}}. \quad (46)$$

III. MEASURING UNTUNED INPUT CIRCUITS WITH UPCONVERSION

In some applications, especially at low frequencies, resonant input circuits are not practical. Instead, a flux signal is measured in an untuned inductive load such as a magnetometer coil. The sensitivity of this readout is often quantified by its imprecision, uncoupled ‘‘energy sensitivity,’’ which expresses the smallest current signal that can be detected above the imprecision noise for a given inductance [30]. In the case of an untuned circuit, the impedance of the input circuit is so high that backaction noise is insignificant. In this case, the only limit on the noise is set by the fluctuations in the imprecision quadra-

ture $\hat{\delta}_{imp}$, and the final noise temperature is determined by the precision of the phase estimation, as determined by the standard quantum limit on interferometry [31].

We can express the energy sensitivity of an upconverter operated with an untuned input circuit as:

$$\epsilon = \frac{\bar{S}_{II} L_b}{2}, \quad (47)$$

where L_b is the self inductance of the input coil which couples flux from the low-frequency circuit into the interferometer. The imprecision energy sensitivity can be expressed as a multiple of \hbar . The details of the operation of dc SQUIDs limits their imprecision energy sensitivity to $\epsilon \gtrsim \hbar$ (see for example [32]), but we emphasize that this is not a standard quantum limit. It is nonetheless the appropriate figure of merit for important applications with untuned input circuits.

In a dc SQUID, the input imprecision current noise can be reduced by increasing the inductance, but this does not change the imprecision energy sensitivity 47. However, in an RQU, the imprecision current noise can be reduced by increasing the pump power $|\bar{a}|^2$, without changing the input inductance, reducing the imprecision energy sensitivity.

Substituting equation 36 into equation 47, we see that at low frequencies ($\omega \ll \kappa/2$), the RQU achieves an imprecision-noise-limited uncoupled energy sensitivity $\epsilon < \hbar$ as long as the amplitude of the microwave drive is larger than:

$$|\bar{a}|^2 > \frac{\omega_b \kappa L_b^2}{16g_0^2 M^2}, \quad (48)$$

suggesting that it may outperform the best dc SQUIDs in some untuned applications. To achieve this performance, the RQU must be designed so that this tone power can be applied without approaching junction critical currents or resonator bifurcation [33].

IV. NUMERICAL ESTIMATES OF RQU PARAMETERS

In order to inform the design of a practical RQU, we introduce an example low frequency resonator. This example resonator has parameters similar to those that are useful in a variety of precision measurement tasks, e.g. searches for low-mass dark matter candidates [16] or high sensitivity measurements of nuclear spin ensembles [7]. There is substantial flexibility in the design of the RQU which would allow the design to be adapted to higher or lower frequency ranges, or broadband experiments, but the example resonator serves as a benchmark for initial RQU designs.

In order to reach the SQL near the low-frequency resonance, the RQU must be driven with a sufficiently strong microwave tone such that its noise impedance (given by equation 41, with a maximum value set in 46) can match

the source impedance of the low frequency resonator, which is entirely determined by its inductance, resonant frequency, and quality factor. We choose a 5 μH inductance as a representative value for a centimeter-scale pickup coil with a few tens of turns (as might be used in a low-mass dark matter experiment searching for electromagnetic [11] or nuclear [34] interactions). We also note that in principle it is possible to use an N -turn step down transformer to lower the pickup coil impedance seen by the RQU by a factor of $1/N$. We do not include this transformer here when evaluating RQU designs, but a transformer might be used to increase the noise impedance further than is achievable with a practical microwave drive tone.

Precisely on-resonance, the impedance of the low-frequency resonator is real, with value

$$R_b = \frac{\omega_b L_b}{Q_b}. \quad (49)$$

In order to reach the SQL, the maximum noise impedance of the RQU must exceed R_b , so that the optimal microwave drive level given in equation 42 can be reached without bifurcation:

$$R_{\max} > \frac{\omega_b L_b}{Q_b}. \quad (50)$$

We can also express this condition as a minimum quality factor Q_{\min} which the low-frequency resonator must achieve in order to be read out at the SQL:

$$Q_{\min} = \frac{\omega_b L_b}{R_{\max}}. \quad (51)$$

For a fiducial RQU design based on a SQUID with an effective critical current $I_c = 5 \mu\text{A}$, we estimate R_{\max} to be 500 $\mu\Omega$, yielding value $Q_{\min} \approx 62,000$, a reasonable Q for a superconducting resonator constructed with low-loss materials in this frequency range, e.g. [35].

V. TWO-TONE MICROWAVE DRIVES

The single-tone microwave drive scheme above makes the RQU operate as a linear, phase-insensitive op-amp, subject to the SQL on amplification. Quantum metrology, including measurements better than the SQL, are enabled by more sophisticated drive schemes. In this section we analyze the RQU when the microwave drive signal consists of two tones, symmetrically detuned above and below the microwave resonance, which can be used to implement quantum backaction evasion.

The two-tone microwave drive is given by:

$$\bar{a}_{\text{in}} = a_{\text{drive}} \sin(\omega_b t + \phi_{\text{drive}}) e^{i\omega_a t}, \quad (52)$$

where a_{drive} specifies the amplitude of the two-tone drive, and ϕ_d sets the phase of the amplitude modulation. Without loss of generality, we can set $\phi_d = 0$. Solving for

the classical amplitude of the field within the microwave resonator yields:

$$\bar{a} = a_{\max} \cos(\omega_b t + \delta) e^{-i\omega_a t}, \quad (53)$$

where a_{\max} captures the rung-up amplitude of the modulated microwave tone:

$$a_{\max} = a_{\text{drive}} \sqrt{\frac{\kappa}{\kappa^2 + 4\omega_b^2}}, \quad (54)$$

and δ encodes the phase of the amplitude modulation envelope:

$$\delta = \arctan(\kappa/\omega_b). \quad (55)$$

Since the RQU biased this way functions as a phase-sensitive amplifier, it is more useful to define the state of the low-frequency resonator by its quadrature operators:

$$\hat{X} = \frac{1}{\sqrt{2}}(\hat{b}e^{i\omega_b t} + \hat{b}^\dagger e^{-i\omega_b t}), \quad (56)$$

$$\hat{Y} = \frac{-i}{\sqrt{2}}(\hat{b}e^{i\omega_b t} - \hat{b}^\dagger e^{-i\omega_b t}) \quad (57)$$

We can calculate the equations of motion for \hat{X} and \hat{Y} , following the derivation in [21]. We find that the total noise spectral density of the measured \hat{X} quadrature is given by:

$$S_X(\omega) = \frac{\gamma/2}{\omega^2 + (\gamma/2)^2} (1 + 2(n_{\text{eq}} + n_{\text{bad}})), \quad (58)$$

where n_{eq} describes the thermal occupation of the low-frequency resonator and n_{bad} describes the spurious backaction on the ideally backaction-free \hat{X} quadrature:

$$n_{\text{bad}} = \frac{(a_{\max} g_0 \Phi_{ZPF})^2}{16\kappa\gamma} \left(\frac{\kappa}{\omega_b}\right)^2. \quad (59)$$

In the limit of good sideband resolution $\omega_b/\kappa \gg 1$, this spurious backaction can be arbitrarily suppressed, corresponding to a backaction-free, or quantum non-demolition (QND) measurement. In this scheme, the RQU can operate at high microwave power levels, reducing imprecision noise on the \hat{X} quadrature, without the backaction penalty present in the single-tone, phase-insensitive mode of operation (as captured by the backaction voltage term in equation 37). This backaction-free measurement mode could allow a quantum speedup in dark matter searches.

VI. RQU UPCONVERSION DEMONSTRATION

We demonstrate RQU operation as both a phase-insensitive amplifier (with one tone on resonance, shown schematically in figure 2), and as a phase-sensitive amplifier (with two pump tones symmetrically detuned on

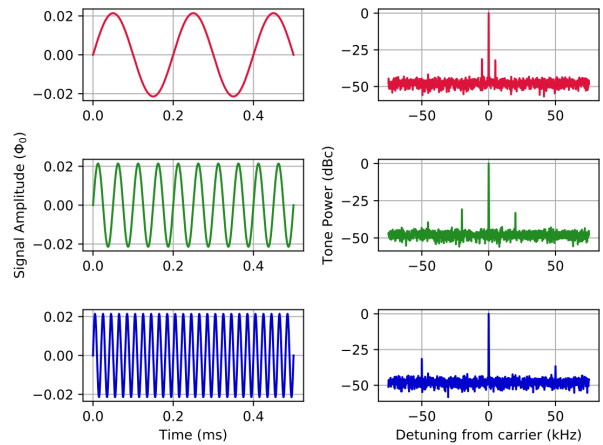


FIG. 2. Data demonstrating phase-insensitive upconversion, showing the strong carrier tone used to bias the RQU at $\Delta \sim 0$ and the two weak signal sidebands, for a variety of different frequencies of the flux signal Φ_b .

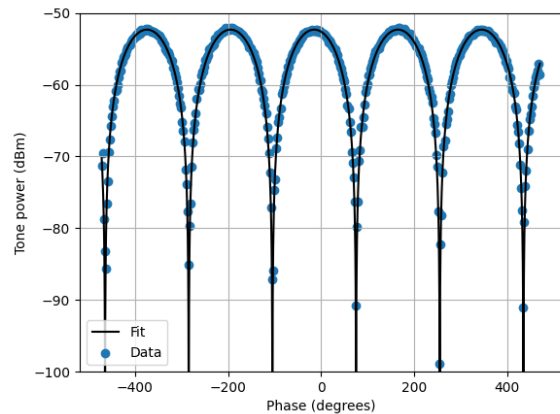


FIG. 3. A demonstration of phase-sensitive upconversion, with a 46.9 dB phase-sensitive extinction ratio. The data are fit to a model with only the amplitude and phase as free parameters.

either side of the microwave resonance, shown in figure 3), using a quarter-wave microwave resonator with a single-junction SQUID at the current antinode providing flux tunability.

In order to demonstrate phase-sensitive readout, two tones are synthesized in separate microwave generators and combined in a power splitter. A shared 10MHz clock source allowed the microwave synthesizers, a low-frequency function generator, and a microwave spectrum analyser to generate and detect phase-coherent tones, which drive the upconverter.

Figure 4, shows a schematic of the setup, in which an RQU is operated at $T \sim 300\text{mK}$ at the base stage of a ^3He sorption cryostat. Filtered and attenuated microwave lines allow for low-noise microwave probe tones

to interrogate the RQU, and a High Electron Mobility Transistor (HEMT) amplifier provides low-noise amplification of the tones that transmit past the RQU. A filtered and attenuated twisted-pair line provides flux bias to the SQUID loop of the RQU, allowing for signals up to a few MHz.

We generate tones symmetrically detuned by 2.9MHz from the 4.89 GHz resonance frequency of the upconverter. We also use the flux bias to modulate the SQUID at 2.9 MHz, and sweep the phase of the SQUID modulation tone over approximately 1080 degrees. The spectrum of the transmitted microwave tones is recorded at a spectrum analyzer. As the phase of the flux modulation changes with respect to the envelope defined by the beating of the microwave tones changes, the total power upconverted modulates, showing a phase-sensitive extinction ratio of 46.9 dB.

The high extinction ratio proves the viability of phase-sensitive upconversion, although it does not constitute a full backaction-evading measurement, which will require a high-Q resonant circuit on the input of the upconverter. For this signal frequency and this upconverter, the spurious backaction terms n_{bad} would have limited the degree of backaction evasion to less than 10dB, in any case. However, reducing the microwave loss rate κ by increasing the microwave quality factor can reduce the spurious backaction, in principle arbitrarily.

VII. CONCLUSIONS

The RQU a tool for quantum metrology of low-frequency electromagnetic modes. We have shown that this interaction allows the RQU to act as a quantum-limited op-amp with tunable noise impedance. Using the RQU as a replacement for dc SQUIDs enables amplification at the SQL and *in situ* tunable noise impedance. Furthermore, the RQU can achieve an uncoupled “energy sensitivity” $(1/2)L_{in}S_I$ significantly below \hbar when coupled to an untuned input inductor. Such performance is not possible with a dc SQUID in which L_{in} is linked to S_I [30]. These functions are useful in a variety of magnetometry applications.

The RQU can also be operated as a phase-sensitive amplifier, enabling performance beyond the SQL via backaction evading measurements, which has the potential to dramatically enhance the performance of an important class of fundamental physics experiments. We have demonstrated the basic functionality of upconversion in both phase-insensitive and phase-sensitive modes, converting signals from 5kHz to 3MHz into the microwave C band. The phase-sensitive data has an extinction ratio of 46.9dB, which is a necessary step

towards achieving a high degree of backaction evasion in future experiments. This will enable beyond-SQL metrology in a variety of precision experiments, including searches for sub- μ eV axion dark matter.

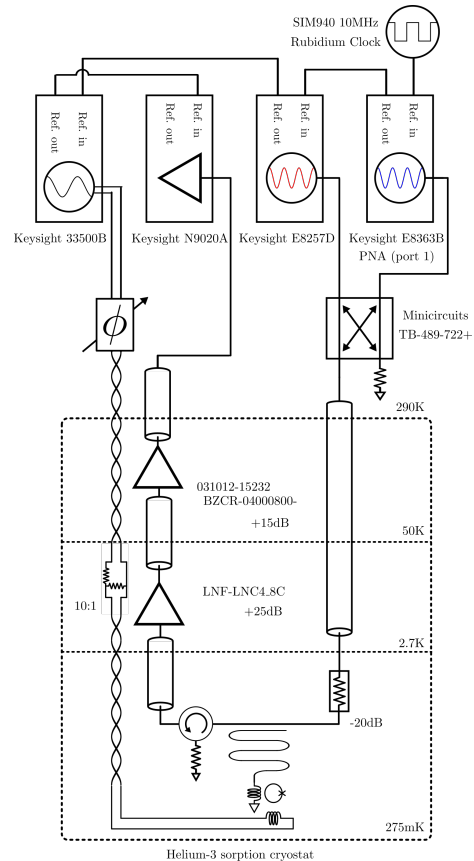


FIG. 4. The microwave and cryogenic setup used to demonstrate phase-sensitive upconversion. The RQU is at the base stage of a helium-3 sorption cryostat, with a 4-8GHz microwave readout chain.

VIII. ACKNOWLEDGMENTS

This work was supported by the US Department of Energy, Office of High Energy Physics program under the QuantISED program, FWP 100667. S. Chaudhuri acknowledges the support of the R.H. Dicke Postdoctoral Fellowship and the David Wilkinson Fund. CY was supported in part by the National Science Foundation Graduate Research Fellowship Program under Grant No. 1656518. Part of this work was performed at the Stanford Nano Shared Facilities (SNSF)/Stanford Nanofabrication Facility (SNF), supported by the National Science Foundation under award ECCS-2026822. Additional microfabrication support was provided by K. Multani, A.Y. Cleland and the Safavi-Naeini group.

- 032329 (2007), ISSN 10502947, URL <https://journals.aps.org/pr/abstract/10.1103/PhysRevA.75.032329>.
- [2] B. R. Johnson, M. D. Reed, A. A. Houck, D. I. Schuster, L. S. Bishop, E. Ginossar, J. M. Gambetta, L. Dicarlo, L. Frunzio, S. M. Girvin, et al., *Nature Physics* **6**, 663 (2010), ISSN 17452481, URL www.nature.com/naturephysics.
- [3] Y. F. Chen, D. Hover, S. Sendelbach, L. Maurer, S. T. Merkel, E. J. Pritchett, F. K. Wilhelm, and R. McDermott, *Physical Review Letters* **107**, 217401 (2011), ISSN 00319007, URL <https://journals.aps.org/prl/abstract/10.1103/PhysRevLett.107.217401>.
- [4] Y. Nakamura, Y. A. Pashkin, and J. S. Tsai, *Nature* **398**, 786 (1999), ISSN 00280836, URL www.nature.com.
- [5] F. Arute, K. Arya, R. Babbush, D. Bacon, J. C. Bardin, R. Barends, R. Biswas, S. Boixo, F. G. Brandao, D. A. Buell, et al., *Nature* **574**, 505 (2019), ISSN 14764687, URL <https://doi.org/10.1038/s41586-019-1666-5>.
- [6] L. Brouwer, S. Chaudhuri, H.-M. Cho, J. Corbin, C. Dawson, A. Droster, J. Foster, J. Fry, P. Graham, R. Henning, et al., *Physical Review D* **106**, 112003 (2022).
- [7] T. Sleator, E. L. Hahn, C. Hilbert, and J. Clarke, *Phys. Rev. Lett.* **55**, 1742 (1985), URL <https://link.aps.org/doi/10.1103/PhysRevLett.55.1742>.
- [8] J. Zmuidzinas, *Applied optics* **42**, 4989 (2003).
- [9] M. F. Gely, M. Kounalakis, C. Dickel, J. Dalle, R. Vatré, B. Baker, M. D. Jenkins, and G. A. Steele, *Science* **363**, 1072 (2019).
- [10] S. Chaudhuri, P. W. Graham, K. Irwin, J. Mardon, S. Rajendran, and Y. Zhao, *Physical Review D - Particles, Fields, Gravitation and Cosmology* **92**, 075012 (2015), ISSN 15502368, URL <https://journals.aps.org/prd/abstract/10.1103/PhysRevD.92.075012>.
- [11] A. Phipps, S. E. Kuenstner, S. Chaudhuri, C. S. Dawson, B. A. Young, C. T. FitzGerald, H. Froland, K. Wells, D. Li, H. M. Cho, et al., in *Microwave Cavities and Detectors for Axion Research Proceedings of the 3rd International Workshop* (Springer Science and Business Media Deutschland GmbH, 2020), vol. 245, pp. 139–145, ISBN 9783030437602, ISSN 18674941, URL https://doi.org/10.1007/978-3-030-43761-9_16.
- [12] J. L. Ouellet, C. P. Salemi, J. W. Foster, R. Henning, Z. Bogorad, J. M. Conrad, J. A. Formaggio, Y. Kahn, J. Minervini, A. Radovinsky, et al., *Physical Review Letters* **122**, 121802 (2019), ISSN 10797114, URL <https://journals.aps.org/prl/abstract/10.1103/PhysRevLett.122.121802>.
- [13] N. Crisosto, P. Sikivie, N. S. Sullivan, D. B. Tanner, J. Yang, and G. Rybka, *Physical Review Letters* **124**, 241101 (2020), ISSN 10797114, URL <https://journals.aps.org/prl/abstract/10.1103/PhysRevLett.124.241101>.
- [14] A. Garcon, D. Aybas, J. W. Blanchard, G. Centers, N. L. Figueroa, P. W. Graham, D. F. Kimball, S. Rajendran, M. G. Sendra, A. O. Sushkov, et al., *Quantum Science and Technology* **3**, 014008 (2018), ISSN 20589565, URL <https://doi.org/10.1088/2058-9565/aa9861>.
- [15] L. H. Nguyen, A. Lobanov, and D. Horns, *Journal of Cosmology and Astroparticle Physics* **2019**, 014 (2019), ISSN 14757516, URL <https://doi.org/10.1088/1475-7516/2019/10/014>.
- [16] S. Chaudhuri, K. Irwin, P. W. Graham, and J. Mardon, arXiv (2018), URL <http://arxiv.org/abs/1803.01627>.
- [17] S. Chaudhuri, K. D. Irwin, P. W. Graham, and J. Mardon, arXiv (2019), URL <http://arxiv.org/abs/1904.05806>.
- [18] M. Reagor, W. Pfaff, C. Axline, R. W. Heeres, N. Ofek, K. Sliwa, E. Holland, C. Wang, J. Blumoff, K. Chou, et al., *Physical Review B* **94**, 014506 (2016), ISSN 24699969, URL <https://journals.aps.org/prb/abstract/10.1103/PhysRevB.94.014506>.
- [19] A. Roy and M. Devoret, *Comptes Rendus Physique* **17**, 740 (2016), ISSN 16310705.
- [20] M. A. Castellanos-Beltran, K. D. Irwin, G. C. Hilton, L. R. Vale, and K. W. Lehnert, *Nature Physics* **4**, 928 (2008), ISSN 17452481, URL www.nature.com/naturephysics.
- [21] A. A. Clerk, F. Marquardt, and K. Jacobs, *New Journal of Physics* **10**, 95010 (2008), ISSN 13672630, URL <http://www.njp.org/>.
- [22] M. Aspelmeyer, T. J. Kippenberg, and F. Marquardt, *Reviews of Modern Physics* **86**, 1391 (2014), ISSN 15390756, URL <https://journals.aps.org/rmp/abstract/10.1103/RevModPhys.86.1391>.
- [23] J. Mates, G. C. Hilton, K. D. Irwin, L. R. Vale, and K. Lehnert, *Applied Physics Letters* **92** (2008).
- [24] E. M. Levenson-Falk, R. Vijay, N. Antler, and I. Siddiqi, *Superconductor Science and Technology* **26**, 055015 (2013), URL <https://dx.doi.org/10.1088/0953-2048/26/5/055015>.
- [25] R. Lescanne, M. Villiers, T. Peronin, A. Sarlette, M. Delbecq, B. Huard, T. Kontos, M. Mirrahimi, and Z. Leghtas, *Nature Physics* **16**, 509 (2020).
- [26] D. F. Walls and G. J. Milburn, *Quantum optics* (Springer Berlin Heidelberg, 2008), ISBN 9783540285731.
- [27] C. M. Caves, *Physical Review D* **26**, 1817 (1982).
- [28] A. A. Clerk, M. H. Devoret, S. M. Girvin, F. Marquardt, and R. J. Schoelkopf, *Reviews of Modern Physics* **82**, 1155 (2010), ISSN 00346861, URL <https://journals.aps.org/rmp/abstract/10.1103/RevModPhys.82.1155>.
- [29] C. Laffamme and A. A. Clerk, *Phys. Rev. A* **83**, 033803 (2011), URL <https://link.aps.org/doi/10.1103/PhysRevA.83.033803>.
- [30] R. F. Voss, *Applied Physics Letters* **38**, 182 (1981), ISSN 00036951, URL <http://aip.scitation.org/doi/10.1063/1.92271>.
- [31] L. Pezzé, A. Smerzi, G. Khoury, J. F. Hodelin, and D. Bouwmeester, *Phys. Rev. Lett.* **99**, 223602 (2007), URL <https://link.aps.org/doi/10.1103/PhysRevLett.99.223602>.
- [32] R. H. Koch, D. J. V. Harlingen, and J. Clarke, *Applied Physics Letters* **38**, 380 (1981), ISSN 00036951, URL <http://aip.scitation.org/doi/10.1063/1.92345>.
- [33] V. E. Manucharyan, E. Boaknin, M. Metcalfe, R. Vijay, I. Siddiqi, and M. Devoret, *Physical Review B - Condensed Matter and Materials Physics* **76**, 014524 (2007), ISSN 10980121, URL <https://journals.aps.org/prb/abstract/10.1103/PhysRevB.76.014524>.
- [34] D. Aybas, J. Adam, E. Blumenthal, A. V. Gramolin, D. Johnson, A. Kleyheeg, S. Afach, J. W. Blanchard, G. P. Centers, A. Garcon, et al., *Phys. Rev. Lett.* **126**, 141802 (2021), URL <https://link.aps.org/doi/10.1103/PhysRevLett.126.141802>.
- [35] S. E. Kuenstner, Ph.D. thesis, Stanford University (2022), copyright - Database copyright ProQuest LLC; ProQuest does not claim copyright in the individual underlying works; Last updated - 2024-03-20.